INTERNATIONAL JOURNAL FOR NUMERICAL AND ANALYTICAL METHODS IN GEOMECHANICS
Int. J. Numer. Anal. Meth. Geomech. 2015; **39**:507–523
Published online 9 September 2014 in Wiley Online Library (wileyonlinelibrary.com). DOI: 10.1002/nag.2320

Uniform investigation of hydraulic fracturing propagation regimes in the plane strain model

J.Q. Bao*,†, E. Fathi and S. Ameri

Department of Petroleum and Natural Gas Engineering, West Virginia University, Morgantown, WV 26506, U.S.A.

SUMMARY

The hydraulic fracturing propagation regimes in the plane strain model are uniformly investigated using a numerical method based on the finite element method. The regimes range from toughness-dominated cases to viscosity-dominated cases, covering zero leak-off situations and small leak-off situations. Unlike the asymptotic solutions, the numerical method is independent of the energy dissipation regimes and fluid storage regimes. The numerical method pays no special attention to the fracture tip, and it simulates fracture tip behaviors by increasing the number of functions in a natural and uniform manner. The numerical method is verified by comparing its results with the asymptotic solutions. The effect of the model sizes on the numerical method is discussed along with the robustness of the numerical method. Copyright © 2014 John Wiley & Sons, Ltd.

Received 22 June 2013; Revised 30 June 2014; Accepted 4 July 2014

KEY WORDS: hydraulic fracturing; finite element method; fracture toughness; fluid viscosity; leak off

1. INTRODUCTION

Hydraulic fracturing is a complicated coupled process, where fracture propagation in a solid medium is driven by pressurized fluid. Apart from natural occurrences such as magma-driven dikes [1], hydraulic fracturing is also applied in industry. The applications include the underground storage of hazardous material [2], the measurement of *in situ* stresses [3], barrier walls used to prevent the transport of containment [4], heat production from geothermal reservoirs [5], and the improvement of fossil fuel recovery [6].

The complicated coupled process of hydraulic fracturing involves the nonlocal relationship between the fracture width and the net pressure in the fracture and the nonlinear dependence of the fluid flow within the fracture on the fracture width. The coupled process is accompanied by leak off, which is history dependent, and fracture propagation, which gives rise to continual configuration variations. These four behaviors lead to a variety of hydraulic fracturing propagation regimes, which depend on material parameters and fracture configurations. Simplified hydraulic fracturing models have been developed, which can be used to study the influence of various material parameters [7]. These models include the plane strain [8], PKN [9], and axisymmetric penny-shaped models [10].

In the plane strain model, hydraulic fracturing propagation regimes are controlled by two parameters: K_m and C_m. K_m is used to distinguish the energy dissipation regimes, and C_m is used to distinguish the storage regimes of the injected fluid. A large K_m indicates that the energy dissipated in the viscous fluid is marginal compared with that dissipated by the fracture extension, and the hydraulic fracturing is referred to as a toughness-dominated regime. For a viscosity-dominated regime, however, K_m is small, and the energy is mainly consumed by the viscous fluid flow [11].

*Correspondence to: J. Q. Bao, Department of Petroleum and Natural Gas Engineering, West Virginia University, Morgantown, WV 26506, U.S.A.
†E-mail: bjq05@mails.tsinghua.edu.cn

C_m usually evolves from zero to infinity if the leak-off coefficient is nonzero. In most applications of hydraulic fracturing, the fluid is expected to be mainly stored in the fracture, and C_m is expected to be smaller than 1.0.

Great achievements have been made to obtain asymptotic solutions for some regimes in the plane strain model. The key issue in constructing asymptotic solutions is capturing the correct fracture tip behaviors because they control the global response of the fluid-driven fracture and because they are regime dependent [12]. These asymptotic solutions are classified into the toughness-dominated [13, 14], intermediate [15], and viscosity-dominated solutions [7, 11, 16], and they can be further classified based on C_m. The asymptotic solutions are regime dependent, and they have good accuracy only if the material properties fall into their ranges. Although Spence and Sharp [17] proposed a regime-independent asymptotic solution for an arbitrary K_m, leak off is not considered in their asymptotic solution, and fracture toughness is not prescribed as an input material parameter [18]. A uniform framework that incorporates all the asymptotic solutions does not yet exist [7], although all these asymptotic solutions have the same theoretical backgrounds and assumptions.

It is possible to use numerical methods to investigate hydraulic fracturing propagation regimes in a uniform manner. The common numerical method for hydraulic fracturing is the displacement discontinuity method [19–23], which is a variant of the boundary element method [24]. Great efforts have been made in recent years to investigate hydraulic fracturing propagation regimes using the finite element method, as the finite element method can overcome the limitations that are imposed on the boundary element method [25]. Chen *et al.* [26] and Chen [27] used a finite element method and investigated the toughness-dominated and viscosity-dominated regimes in impermeable mediums (zero leak off), respectively. Carrier and Granet [28] also proposed a finite element method to analyze the toughness-dominated regimes and viscosity-dominated regimes in permeable (leak off) and impermeable mediums. The cohesive zone model [29] was used to simulate fracture propagation in these simulations. A critical concern for the cohesive zone model is that a special technique is needed to ensure its numerical stability because there exists negative tangential stiffness in the cohesive constitutive law [30]. Based on linear elastic fracture mechanics (LEFM), Lecampion [25] applied an extended finite element method to simulate hydraulic fracturing and proposed special functions to capture the fracture tip asymptotes. In addition, Hunsweck *et al.* [31] proposed a coupled finite element method and simulated the viscosity-dominated hydraulic fracturing propagation regimes in impermeable mediums. In their simulations, it is assumed that the fluid front never reaches the fracture tip. This assumption is to avoid additional care of addressing the contact condition at the fracture tip [31].

In this paper, an alternative numerical method based on the finite element method is proposed to uniformly investigate the hydraulic fracturing propagation regimes in the plane strain model. A unique feature of the proposed method is that no special attention is paid to the fracture tip, whether the propagation regimes are viscosity dominated, intermediate, or toughness dominated and whether the solid medium is permeable.

The proposed method shares the same theories and assumptions as the aforementioned asymptotic solutions. The theories include LEFM for fracture propagation, lubrication theory for the fluid flow within the fracture [32], and Carter's leak-off model [33]. The assumptions include uniform confining stress, zero gap between the fluid front within the fracture and the fracture tip, and a straight fracture propagation path that is perpendicular to the confining stress.

We focus our investigation on cases with C_m ranging from 0 to 1, although the proposed method has no simplification or assumption related to C_m and is applicable to cases with any C_m. The rest of this paper is organized as follows: The theoretical model of hydraulic fracturing is presented in section 2. The hydraulic fracturing propagation regimes in the plain strain model, as well as some asymptotic solutions, are briefly introduced in section 3. The proposed numerical method is described in section 4. The investigation, the comparisons of numerical results with asymptotic solutions, and some discussions are presented in section 5. Some conclusions are made in section 6.

2. THEORETICAL MODELS

A hydraulic fracture, which is driven by the injection of an incompressible Newtonian fluid at a constant rate and propagates in an isotropic and homogeneous solid medium, is considered in this

DOI: 10.1002/nag

paper. Based on LEFM, the fracture propagation is related to the material parameters of the solid, which are the elastic modulus E, Poisson's ratio v, and fracture toughness K_{IC}. Let Q_0 denote the constant injection rate as shown in Figure 1, μ denote the dynamic viscosity of the fluid, and C_l denote the leak-off coefficient. For convenience, new parameters are defined as

$$E' = \frac{E}{1-v^2}, \quad K' = 4\left(\frac{2}{\pi}\right)^{1/2} K_{IC}, \quad \mu' = 12\mu, \quad C_l' = 2C_l. \tag{1}$$

The confining stress σ_0 as shown in Figure 1 is positive when it is compressive. Because σ_0 is uniform, the fracture profile is symmetric in the x direction, with the center located at the inlet, that is, the injection point. The relationship between the fracture width w and the net fluid pressure p at any moment t in the half space ($x \geq 0$) can be expressed as [24]

$$w(x,t) = \frac{\pi}{4E'} \int_{l_t} \ln \left| \frac{\sqrt{l_t^2 - x^2} + \sqrt{l_t^2 - x_1^2}}{\sqrt{l_t^2 - x^2} - \sqrt{l_t^2 - x_1^2}} \right| p(x_1, t) dx_1, \tag{2}$$

where l_t is the half fracture length at time t, as shown in Figure 1, and the net pressure p satisfies

$$p(x,t) = p_f(x,t) - \sigma_0(x), \tag{3}$$

where p_f is the fluid pressure. It is observed in Eqns (2) and (3) that the net pressure rather than the fluid pressure contributes to the fracture width. It is clear that the fracture is also symmetric in the y direction. Therefore, the model in Figure 1 can be represented by its equivalent quarter model as shown in Figure 2, where the net pressure is applied on the fracture surface.

The fracture propagation criterion is

$$K_I = K_{IC}, \tag{4}$$

where K_I is the stress intensity factor of the Griffith crack [24]. When K_I reaches K_{IC} at the fracture tip, the near-tip fracture width can be approximated by [34]

$$w(x) = \frac{K'}{E'}(l_t - x)^{1/2} + O\left[(l_t - x)^{3/2}\right], \; l_t - x << l_t. \tag{5}$$

The mass conservation of the injected fluid leads to

$$\frac{\partial w}{\partial t} + g = -\nabla \cdot \boldsymbol{q}, \tag{6}$$

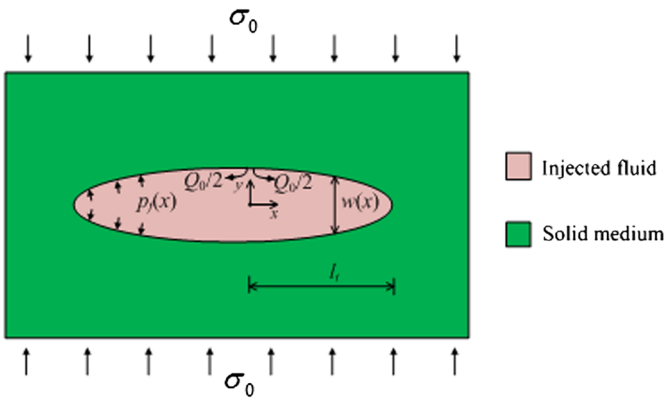

Figure 1. Sketch of a plane strain, fluid-driven fracture.

DOI: 10.1002/nag

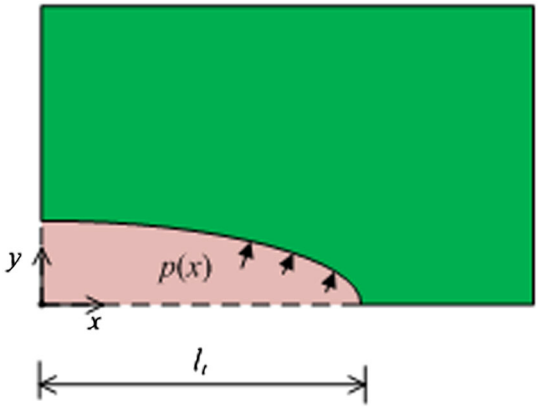

Figure 2. Equivalent quarter model.

where g is the leak off, $\nabla\cdot$ is the divergence operator, and $\boldsymbol{q}$ is the fluid flux. It is observed in Eqn (6) that the injected fluid flowing through the fracture is divided into two parts. The first part stays in the fracture and contributes to fracture width variations, and the second part leaks into the solid medium.

The fluid flow within the fracture is modeled using lubrication theory. Thus, the relationship between the fluid flux $\boldsymbol{q}$ and the fracture width w is given by Poiseuille's law [32]:

$$\boldsymbol{q} = -\frac{w^3}{\mu'}\nabla p_f, \tag{7}$$

where ∇ is the gradient operator. The leak off is characterized by Carter's model [33] as

$$g(x,t) = C_l'/\sqrt{t - t_0(x)}, \quad t > t_0(x), \tag{8}$$

where t_0 is the fracture tip arrival time. Because the confining stress is uniform Eqn (7) can be replaced by

$$\boldsymbol{q} = -\frac{w^3}{\mu'}\nabla p. \tag{9}$$

The divergence and gradient operators in Eqns (6), (7), and (9) are defined in the fracture propagation direction, that is, the x direction in Figure 2.

The boundary conditions for fluid flow within the fracture are

$$\boldsymbol{q}(x = 0^+, t) = Q_0/2, \boldsymbol{q}(x = l_t,\ t) = 0. \tag{10}$$

The first boundary condition in Eqn (10) is from the symmetry of the biwing fracture as shown in Figure 1. The second boundary condition in Eqn (10) originates from the zero fracture width at the fracture tip [7].

Using the divergence theorem [35], Eqn (6) combined with the boundary conditions in Eqn (10) and the leak-off model in Eqn (8) leads to the global fluid continuity equation [15]

$$\int_0^{l_t} w(x,t)dx + \int_0^t \int_0^{l_{t'}} g(x,t')dxdt' = \frac{1}{2}Q_0 t. \tag{11}$$

Based on Eqn (11), the injection efficiency η, which is the volume ratio of the fluid that remains in the fracture to the injected fluid, is defined as

$$\eta(t) = \int_0^{l_t} w(x,t)dx \Big/ \left[\frac{1}{2}(Q_0 t)\right]. \tag{12}$$

DOI: 10.1002/nag

3. HYDRAULIC FRACTURING REGIMES AND ASYMPTOTIC SOLUTIONS

Hydraulic fracturing regimes in the plane strain model are constructed using a rectangular phase diagram $M\tilde{M}K\tilde{K}$ as shown in Figure 3 in (K_m, C_m) space [14]. For a constant injection rate, K_m and C_m are defined as [15]

$$K_m = \frac{K'}{E'}\left(\frac{E'}{\mu' Q_0}\right)^{1/4}, \quad C_m = C'\left(\frac{E' t}{\mu' Q_0^3}\right)^{1/6}. \tag{13}$$

K_m and C_m are used to differentiate the energy dissipation regimes and the fluid storage regimes, respectively. It is observed in Eqn (13) that K_m is time independent and C_m is time dependent. C_m always evolves from zero to infinity along a straight evolution line as shown in Figure 3, if the leak-off coefficient is nonzero. This means that in the beginning the fluid is mainly stored in the fracture, and the injection efficiency is close to 1; subsequently, the injection efficiency decreases.

Hydraulic fracturing propagation regimes can be categorized into the toughness-dominated, intermediate, and viscosity-dominated regimes based on K_m. The regimes are toughness dominated if the K_ms are larger than 4.0 and are viscosity dominated if the K_ms are smaller than 1.0; otherwise, they are intermediate [15].

Hydraulic fracturing regimes can be presented through the introduction of a scaling technique [15], which transforms the variables p, w, and l_t into dimensionless variables Π, Ω, and γ, respectively. The variables Π and Ω are functions of the dimensionless coordinate ξ, which ranges from 0 at the inlet to 1 at the fracture tip. The scaling technique has the advantage of reducing the variables in the hydraulic fracturing regimes to dimensionless quantities of order 0(1) whenever possible [15] and relieving the burden of constructing the asymptotic solutions. The key issue for the determination of the asymptotic solutions is constructing appropriate tip asymptotes [12]. Some of the asymptotic solutions are briefly introduced as follows.

3.1. K and M vertex solutions

The K vertex regime corresponds to the case of zero fluid viscosity and zero leak off. The K vertex solution has a uniform net pressure, and the second term on the right-hand side of Eqn (5) is zero. Therefore, the fracture tip width has an asymptote of $(1-\xi)^{1/2}$. In the K vertex solution [13], the dimensionless opening is defined as

$$\Omega(\xi) = \pi^{-1/3}\left(1-\xi^2\right)^{1/2}. \tag{14}$$

The M vertex regime corresponds to the case of zero fracture toughness and zero leak off, and the second term on the right-hand side of Eqn (5) plays an important role. The near-tip fracture width has the asymptote of [7]

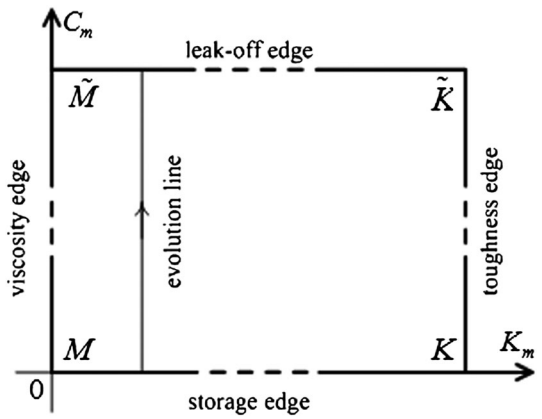

Figure 3. Hydraulic fracturing regimes in (K_m, C_m) space and their evolution line (after Bunger, Detournay, and Garagash [14]).

DOI: 10.1002/nag

$$\Omega(\xi) \sim (1-\xi)^{2/3}. \tag{15}$$

The M asymptotic solution [16] is found by approximating Ω with a series of weighted Gegenbauer polynomials [36], where the weighted function has the form of $(1-\xi^2)^{2/3}$.

3.2. Near-K and near-M solutions

The asymptotic solutions for the near-K and near-M regimes, where there is no leak off, are collectively denoted as $F(\xi) = \{\Omega(\xi),\ \Pi(\xi),\ \gamma\}$. The n-order approximation of the self-similar $F(\xi)$ is

$$F(\xi) = \sum_{i=0}^{n} C^i F_i(\xi), F_i(\xi) = \{\Omega_i(\xi),\ \Pi_i(\xi),\ \gamma_i\}, \tag{16}$$

where C equals K_m^{-4} for the near-K asymptotic solutions [13] and C equals K_m for the near-M asymptotic solutions [11]. The K and M vertex asymptotic solutions are the zeroth-order approximations of the near-K and near-M asymptotic solutions, respectively.

3.3. $K\widetilde{K}$ and $M\widetilde{M}$ edge solutions

The $K\widetilde{K}$ edge regimes correspond to the case of zero fluid viscosity with leak off evolving from zero to infinity. The net pressure is uniform at any given time. Similar to the K vertex solution, the $K\widetilde{K}$ edge solutions [14] also have the property of self-similarity, and the fracture tip always has the asymptote of $\Omega \sim (1-\xi)^{1/2}$.

For the $M\widetilde{M}$ edge regimes, the tip behaviors evolve from $\Omega \sim (1-\xi)^{2/3}$ at small leak off to $\Omega \sim (1-\xi)^{5/8}$ at large leak off [7]. The transient solution is achieved using the application of an explicit finite difference scheme in a moving spatial grid and the displacement discontinuity method with constant-strength dislocations [7].

3.4. Intermediate solutions

In the intermediate solutions [15], the net pressure function Π is proposed to have the form of

$$\Pi = \Pi_L + \Pi_s, \tag{17}$$

where Π_L is a piecewise linear function and Π_s is a singular function that has the form of $\ln(1-\xi^2)$. Π_s is proposed based on the analysis of the fracture tip behavior. The solutions are found using the method of lines [13].

4. FINITE ELEMENT METHODS

4.1. Elastic response

Discretizing the equivalent model using finite elements as shown in Figure 4, we can achieve a finite element equation that describes the elastic behavior of the solid medium, which is cast as

$$\boldsymbol{K}_u \Delta \boldsymbol{U} = \Delta \boldsymbol{F}, \tag{18}$$

where $\mathbf{K}_u$ is the global assembly of the stiffness of the finite elements, $\Delta \boldsymbol{U}$ is the vector of the node displacement increments, and $\Delta \boldsymbol{F}$ is the vector of the equivalent node forces caused by the net pressure increments, that is, Δp as shown in Figure 4.

Because only net pressure increments contribute to $\Delta \boldsymbol{F}$, Eqn (18) can be rewritten as

$$\boldsymbol{K}_u \Delta \boldsymbol{U} = \boldsymbol{B} \Delta \boldsymbol{P}, \tag{19}$$

DOI: 10.1002/nag

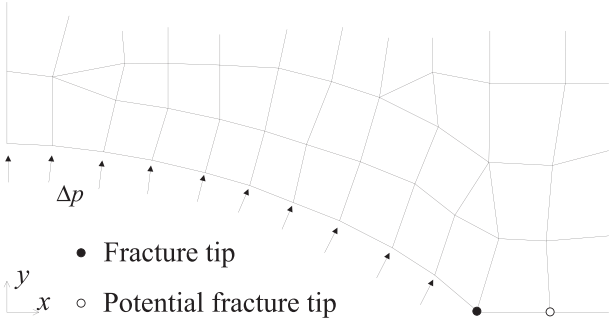

Figure 4. Discretization of the equivalent quarter model with finite elements.

where $\Delta \boldsymbol{P}$ is a vector formed by the pressure increments of nodes on the fracture surface and the matrix $\boldsymbol{B}$ is used to transform the net pressure increments into equivalent node forces.

The interaction integral method [37] is used to calculate K_I. For the plain strain model, K_I is calculated using

$$K_I = E' \left\{ \int_A \left[\sigma_{ij} \frac{\partial u_i^a}{\partial x_1} + \sigma_{ij}^a \frac{\partial u_i}{\partial x_1} - \sigma_{mn}^a \varepsilon_{mn} \delta_{1j} \right] \frac{\partial \chi}{\partial x_j} dS - \int_{S_e} \chi p \frac{\partial u_i^a}{\partial x_1} dL \right\}, \tag{20}$$

where the domain A is a set of elements around the fracture tip as shown in Figure 5, S_e is a collection of element edges on the fracture surface that are shown with dashed lines in Fig. 5, σ_{ij} is the stress field, u_i is the displacement field, $x_j (j = 1, 2)$ is the local coordinate, δ is the Kronecker delta, χ is a scalar field, ε_{mn} is the strain field, and σ_{ij}^a and u_i^a are the auxiliary stress and displacement fields, respectively. The analytical solutions of σ_{ij}^a and u_i^a are listed in Appendix A. The Einstein summation convention is used for the repeated indices in Eqn (20).

The characteristic radius r_c of the fracture tip is defined on the domain A, and

$$r_c = \sqrt{A_{tip}}, \tag{21}$$

where A_{tip} is the summation of the areas of the elements that share the node on the fracture tip. Elements having node(s) in the semicircle as shown in Figure 5 constitute the domain A. The radius of the semicircle equals r_c. The scalar χ equals 1 on the nodes in the semicircle and zero on the nodes out of the semicircle [31]. Theoretically, the interaction integral is independent of the domain A.

In this paper, it is assumed that the fracture propagation length is determined by the finite element mesh. This means that the node on the fracture tip is freed when K_I is not smaller than K_{IC}, and the fracture extends into the node ahead of the fracture tip. This also means that the node ahead of the fracture tip is always the potential fracture tip, which is shown in Figure 4. Similar assumptions can be found elsewhere [38].

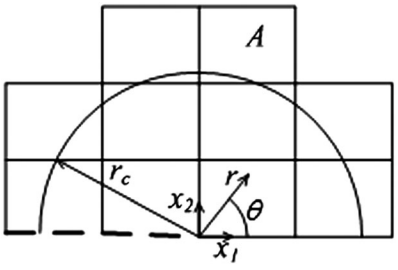

Figure 5. Domain for the interaction integral.

DOI: 10.1002/nag

4.2. Fluid flow within the fracture

Eqn (6) leads to its weak form [23]

$$\int_{l_t}\left[-\nabla(\delta p)\cdot\boldsymbol{q}+(\delta p)\frac{\partial w}{\partial t}+(\delta p)g\right]dl+\delta p(\boldsymbol{q}\cdot n_1)|_S=0, \tag{22}$$

where δp is a testing function and S is a collection of the boundary conditions in Eqn (10). Eqn (22) combined with Eqn (10) leads to a nonlinear finite element equation for the fluid flow within the fracture [23], which is symbolically cast as

$$\boldsymbol{K}_w(\boldsymbol{W})\boldsymbol{P}+\boldsymbol{L}\dot{\boldsymbol{W}}+\boldsymbol{H}=\boldsymbol{0}, \tag{23}$$

where $\mathbf{W}$ is a vector formed by the widths of the nodes on the fracture surface, $\boldsymbol{K}_w(\boldsymbol{W})$ is the assembly of the flux stiffness of the fluid elements, $\boldsymbol{L}$ is the assembly of the length stiffness of the fluid elements, and $\boldsymbol{H}$ includes the contributions of the fluid leak off and the fluid injection.

Taken time integration, Eqn (23) yields

$$\int_{t_n}^{t_{n+1}}\left[\boldsymbol{K}_w(\boldsymbol{W})\boldsymbol{P}+\boldsymbol{L}\dot{\boldsymbol{W}}+\boldsymbol{H}\right]dt=\boldsymbol{0}. \tag{24}$$

A backward Euler scheme for the time difference is used in this paper. Therefore, based on Eqn (24), we have

$$\mathbf{K}_w(\mathbf{W}_{n+1})\mathbf{P}_{n+1}\Delta t-\mathbf{L}(\mathbf{W}_{n+1}-\mathbf{W}_n)+\mathbf{H}\Delta t=\mathbf{0}, \tag{25}$$

where $\boldsymbol{W}_{n+1}$ and $\boldsymbol{P}_{n+1}$ are the unknown fracture widths and net fluid pressures at the $(n+1)$ th step, respectively, $\boldsymbol{W}_n$ is the known fracture width at the nth step, and Δt is the time step between the nth step and the $(n+1)$ th step.

For the $(n+1)$ th step, we have

$$\boldsymbol{W}_{n+1}=\boldsymbol{W}_n+\Delta\boldsymbol{W},\ \boldsymbol{P}_{n+1}=\boldsymbol{P}_n+\Delta\boldsymbol{P}, \tag{26}$$

where $\Delta\boldsymbol{W}$ is a vector formed by the width increments of the nodes on the fracture surface. At any moment, we have

$$\Delta w(x)=2\Delta u_y(x),\ 0\le x\le l_t, \tag{27}$$

where Δu_y is the displacement increment in the y direction on the fracture surface in the equivalent quarter model and Δw is the fracture width increment. Therefore, Eqn (25) can be rewritten in a generalized manner as

$$\boldsymbol{K}_w(\boldsymbol{U}_n+\Delta\boldsymbol{U})(\boldsymbol{P}_n+\Delta\boldsymbol{P})-\boldsymbol{L}'\Delta\boldsymbol{U}+\boldsymbol{H}\Delta t=\boldsymbol{0}, \tag{28}$$

where $\boldsymbol{L}'$ determines the contribution of the node displacement increments to the fracture width increments.

4.3. Solving of the coupled equations

The unknown fracture width increments and the fluid pressure increments at the $(n+1)$ th step can be obtained by solving the coupled Eqns (19) and (28). Although there is no fluid pressure boundary condition for the fluid flow within the fracture, the structure of hydraulic fracturing described by the fluid flow within the fracture, that is, Eqns (6)–(11) and the elastic response of the solid medium is complete [39]. Therefore, the coupled Eqns (19) and (28) are solvable.

The Newton–Raphson iteration algorithm [40, 41] is used to solve the nonlinear coupled equations. In every step, the initial guesses of $\Delta\boldsymbol{W}$ and $\Delta\boldsymbol{P}$ are set to be zero. The following condition is used as the convergence criterion:

DOI: 10.1002/nag

$$\left\|\Delta \boldsymbol{W}^{(m+1)} - \Delta \boldsymbol{W}^{(m)}\right\| / \left\|\Delta \boldsymbol{W}^{(m+1)}\right\| \leq \varepsilon_{tol}, \tag{29}$$

where $\|\ \|$ is the two-norm operator, $\Delta \boldsymbol{W}^{(m+1)}$ and $\Delta \boldsymbol{W}^{(m)}$ are the results of the fracture width increments after the $m+1$th iteration and the mth iteration, respectively, and ε_{tol} is the specified tolerance which equals 1.0e−8 in this paper.

In every step, the stress intensity factor at the fracture tip satisfies

$$K_I \leq \left(1.0 + \varepsilon_{tol}^{s}\right) K_{IC}, \tag{30}$$

where ε_{tol}^{s} is the allowable tolerance for the stress intensity factor, which is taken as 0.001 in this paper. A dynamic time step Δt is used to ensure Eqn (30). One of the advantages of the dynamic time step is that the initial guesses of $\Delta \boldsymbol{W}$ and $\Delta \boldsymbol{P}$ in every step are close to their real solutions.

It is observed that the essential work in the proposed method is in solving the coupled Eqns (19) and (28). No special attention is paid to the fracture tip regardless of the fracture propagation regimes.

5. INVESTIGATION AND DISCUSSION

5.1. Investigation

The plane strain model for this investigation is shown in Figure 6, where a fracture lies horizontally on the left bottom edge. The model is discretized with 2324 linear quad elements and 2523 nodes. Because of the symmetry, edge AB, as shown in Figure 6, is fixed for displacements in the x direction, and edge AD except for the fracture zone is fixed for displacements in the y direction. The characteristic sizes of the elements of the first 15 m of the bottom left edge equal 0.05 m. In our simulations, the fracture propagation path is assumed to be within the first 15 m of the bottom left in the model. The initial half fracture length equals 0.05 m, and the initial net pressure in the fracture is uniform and equals 0.1 MPa.

The investigation includes three cases covering the toughness-dominated, intermediate, and viscosity-dominated regimes. There are two examples in each case: one without leak off and the other with leak off. The parameters used in the investigation are listed in Table I. For all three leak-off examples, C_m equals 1.00 at 67.83 s.

5.1.1. Toughness-dominated case. For the leak-off example, the injection efficiency equals 0.426 when C_m equals 1 in the numerical result, and it equals 0.406 when C_m equals 1 in the $K\widetilde{K}$ edge solution. Figure 7 illustrates the numerical results and the asymptotic solutions for the toughness-dominated case.

5.1.2. Intermediate case. For the leak-off example, the injection efficiency equals 0.294 when C_m equals 1 in the numerical result, and it equals 0.290 when C_m equals 1 in the intermediate solution. The numerical results and the asymptotic solutions for the intermediate case are plotted in Figure 8.

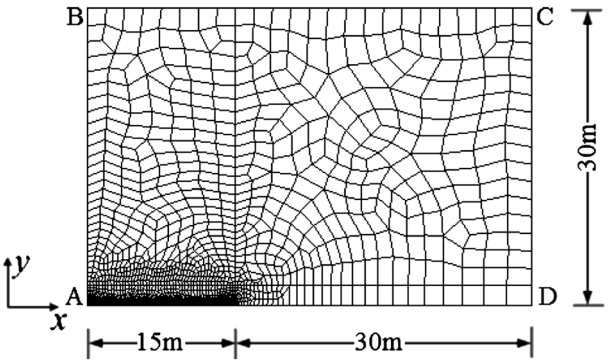

Figure 6. Definition of the model.

DOI: 10.1002/nag

Table I. Parameters for the simulations.

Parameter	Symbol	Value
Elastic modulus	E	18 000 MPa
Poisson' s ratio	v	0.2
Injection rate	Q_0	0.001 m^2/s
Dynamic viscosity	μ	7.98e−7 kPa · s
Fracture toughness	K_{IC}	4 MPa · $m^{1/2}$ (toughness-dominated case, $K_m = 4.53$)
		1.77 MPa · $m^{1/2}$ (intermediate case, $K_m = 2.00$)
		0.25 MPa · $m^{1/2}$ (viscosity-dominated case, $K_m = 0.28$)
Leak-off coefficient	C_l	0.0 (zero-leak-off examples)
		7.0e−5 m · $s^{1/2}$ (leak-off examples)

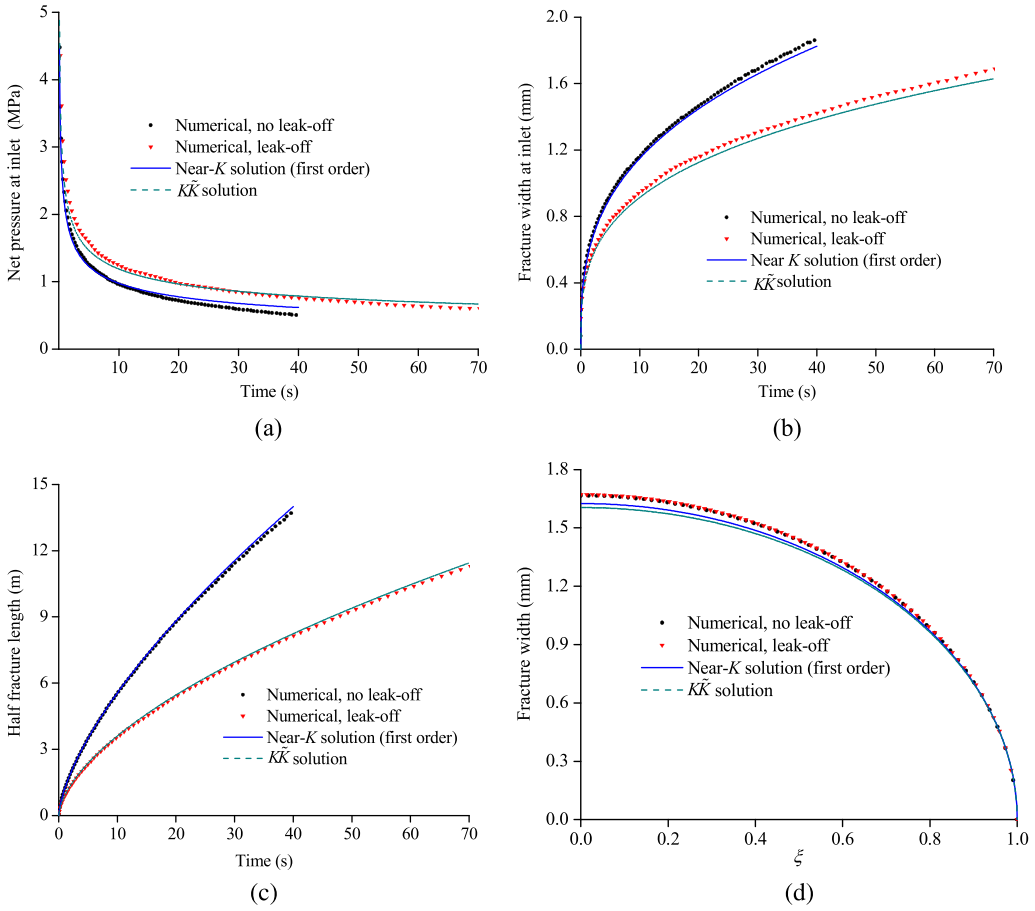

Figure 7. Asymptotic and numerical solutions of the net pressure at the inlet (a), fracture width at the inlet (b), half fracture length (c), and fracture width profile ($l_t = 11.1$ m) (d) for the toughness-dominated case.

5.1.3. Viscosity-dominated case. For the leak-off example, the injection efficiency equals 0.254 when C_m equals 1 in the numerical result, and it equals 0.249 when C_m equals 1 in the $M\tilde{M}$ edge solution. Figure 9 shows the numerical results and the asymptotic solutions for the viscosity-dominated case.

The numerical results and the asymptotic solutions show that for the toughness-dominated and intermediate cases, the leak off has a limited effect on the fracture tip behaviors (Figures 7(d) and 8 (d)), whereas for the viscosity-dominated case, the leak off has a substantial effect on the fracture tip behaviors (Figure 9(d)). The leak-off effects in the numerical method agree well with those in the asymptotic solutions. Although the gaps between the numerical results and the asymptotic solutions

DOI: 10.1002/nag

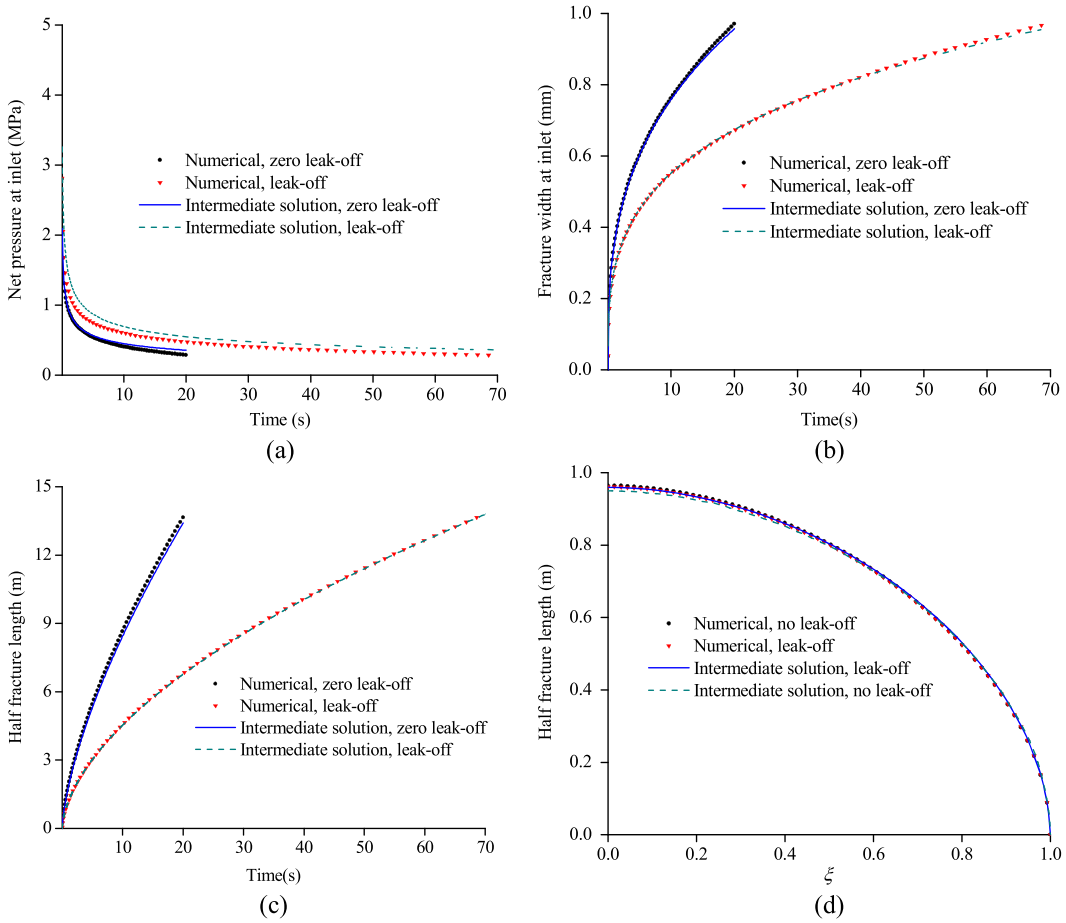

Figure 8. Asymptotic and numerical solutions of the net pressure at the inlet (a), fracture width at the inlet (b), half fracture length (c), and fracture width profile ($l_t = 13.5$ m) (d) for the intermediate case.

in Figures 7–9 increase when the fracture propagates, the numerical results have good accordance with the asymptotic solutions in the six examples when the half fracture length is not longer than 15 m. Because of the accordance, the injection efficiencies obtained using the numerical method match those obtained using the asymptotic solutions. The injection efficiencies of the leak-off example in the intermediate case are plotted in Figure 10. The proposed numerical method is verified.

5.2. *Discussion*

For a constant injection rate, hydraulic fracturing has the property of self-similarity when there is no leak off [17]. To discuss the self-similarity in the proposed numerical method, the virtual net fluid pressure $\widetilde{p}_{l_1}^{l_0}$ is defined as

$$\widetilde{p}_{l_1}^{l_0}(\xi) = \frac{p_{l_0}(0)}{p_{l_1}(0)} p_{l_1}(\xi), \tag{31}$$

where $p_{l_0}(0)$ and $p_{l_1}(0)$ are the net fluid pressure at the inlet when l_t equals l_0 and l_1, respectively, and $p_{l_1}(\xi)$ is the net fluid pressure at ξ when l_t equals l_1. The net fluid pressure profiles $p_{4.0}(\xi)$ in the three zero-leak-off examples in the Investigation subsection are plotted in Figure 11(a), including those obtained using the numerical method and the asymptotic solutions. As in the asymptotic solutions, the net pressure at the fracture tip is singular, and the profiles obtained by the asymptotic solutions are truncated at $\xi = 0.99$. The virtual net fluid pressure profile $\widetilde{p}_{4.0}^{8.0}(\xi)$ and the net fluid pressure

DOI: 10.1002/nag

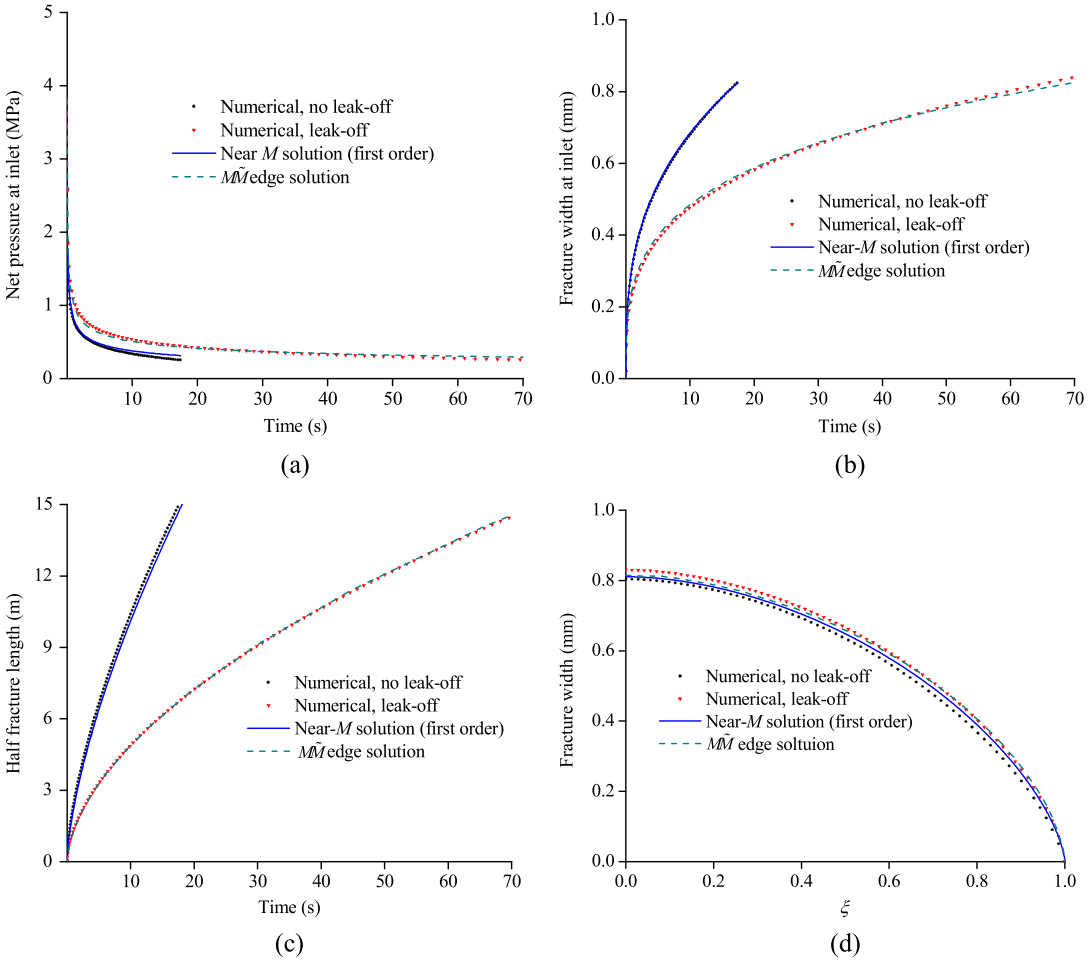

Figure 9. Asymptotic and numerical solutions of the net pressure at the inlet (a), fracture width at the inlet (b), half fracture length (c), and fracture width profile ($l_t = 14.2$ m) (d) for the viscosity-dominated case.

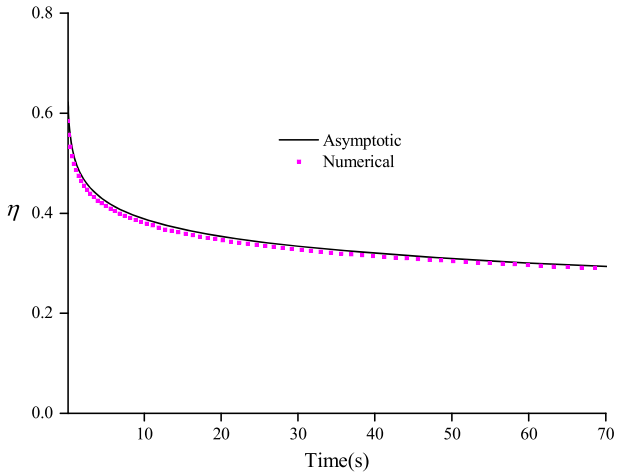

Figure 10. Injection efficiency values for the leak-off example in the intermediate case.

DOI: 10.1002/nag

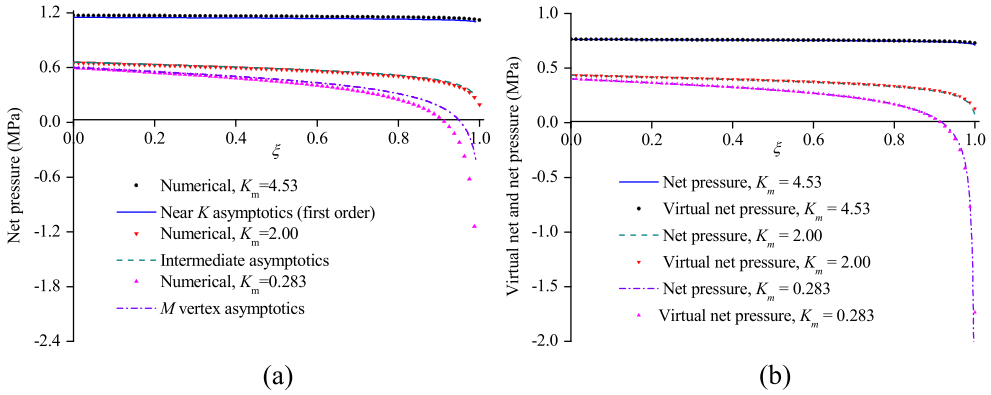

Figure 11. Net pressure profiles with $l = 4$ m (a) and $l = 8$ m (b) and virtual net pressure profiles with $l_0 = 8$ m and $l_1 = 4$ m (b).

profile $p_{8.0}(\xi)$ obtained using the numerical method for the three zero-leak-off examples are plotted in Figure 11(b).

It is observed in Figure 11(a) that the profiles obtained using the numerical method are in excellent agreement with those obtained using the asymptotic solutions for the toughness-dominated and intermediate cases. Although the profile obtained using the numerical method in the viscosity-dominated case is slightly different from that obtained using the asymptotic solution around the zero-net-pressure point, the net pressure around this point has limited contribution to the fracture width. Therefore, the overall numerical results in the viscosity-dominated example match the asymptotic solutions. The good agreements between the net pressure profiles and the virtual net pressure profiles, as shown in Figure 11(b), indicate that the property of self-similarity in hydraulic fracturing is well exhibited by the numerical method.

Although the asymptotic solutions and the numerical method share the same theoretical background, the models in the asymptotic solutions are infinite, whereas the models in the numerical method are finite. Two additional square models are used to analyze the effect of model sizes on the numerical method. The edge lengths of the square models are 120 and 240 m, respectively. The elements in the Investigation subsection can be treated as a set of the elements in the two models. The characteristic sizes of the other elements in the two models are 3.5 m. The left edges of the two models are fixed in the x direction, and the bottom edges, except the fracture zone, are fixed in the y direction. In addition, there are six examples in each model, which have the same material parameters and initial conditions as the examples in the Investigation subsection.

For all the models, the near-K asymptotic solutions and some numerical results of the zero-leak-off examples in the toughness-dominated case are plotted in Figure 12. It is observed in Figure 12 that at the beginning the numerical results are similar to each other and to the asymptotic solution. This is because at the early stage, the fracture is short and the effect of model size is limited. However, when the injection time is greater than 20 s, the effect of the model size becomes more apparent, and the numerical results of the two square models become improved compared with those of the rectangle model.

The relative error of the net pressure at the inlet e_p is defined as

$$e_p = |p_n - p_a|/p_a, \tag{32}$$

where p_n and p_a are the net pressure at the inlet obtained using the numerical method and using the asymptotic solutions at the same simulation time, respectively. The e_ps for the viscosity-dominated examples without leak off in the square and rectangle models are plotted in Figure 13, where the p_as are obtained using the first-order near-M asymptotic solutions. It is observed in Figure 13 that increasing the sizes of the models can effectively increase the accuracy of the numerical method. Similar tendencies are also found in other cases. This means that model difference is one of the leading sources that lead to the difference between the numerical results and the asymptotic solutions. This fact is also found in other examples.

DOI: 10.1002/nag

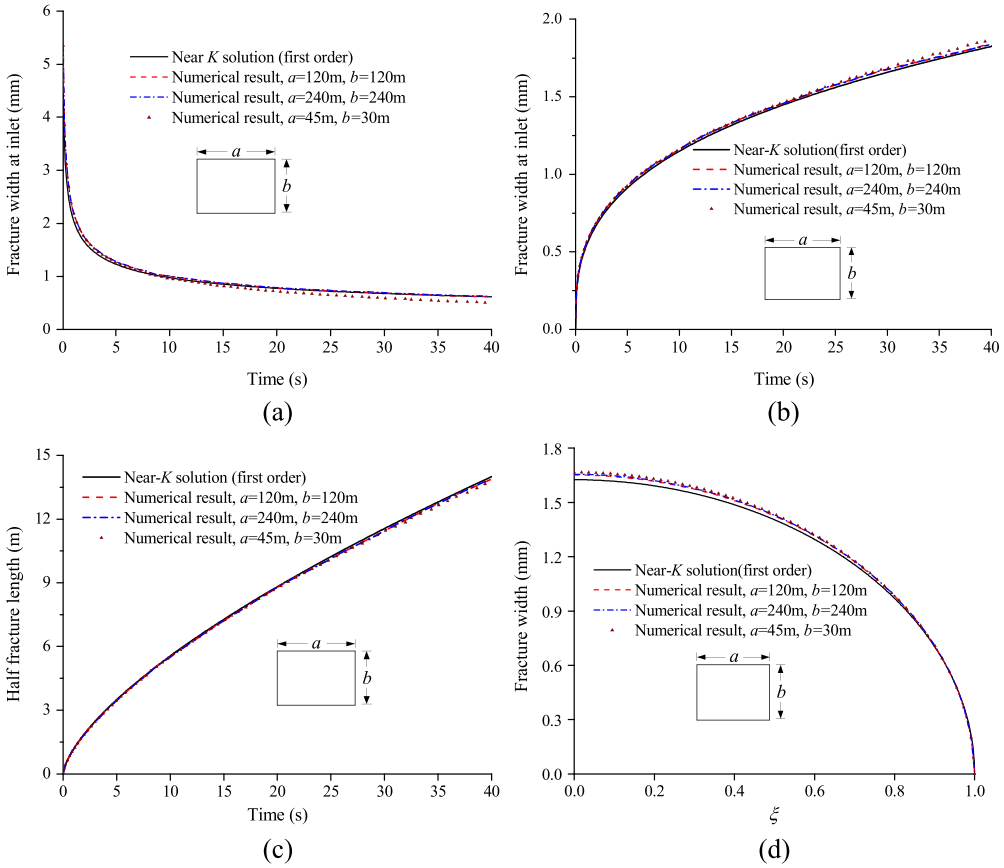

Figure 12. Asymptotic and numerical solutions of the net pressure at the inlet (a), fracture width at the inlet (b), half fracture length (c), and fracture width profile ($l_t = 11.1$ m) (d) of the toughness-dominated examples without leak off.

Taking the zero-leak-off simulations as examples, we explain why special care regarding the fracture tip is not needed in the proposed method. Both the numerical results and the asymptotic solutions in Figure 11(a) show that the net pressure profile can be divided into two zones for a finite K_m: one with smooth gradients of the net pressure and the other with sharp gradients around the fracture tip. Let l_t^{sp} denote the length of the sharp gradient zone in the half fracture at moment t. For a specific criterion that is to differentiate between the two zones, the ratio of l_t^{sp} to l_t is constant because the net pressure profile is self-similar. For the asymptotic solutions and the numerical method, the key point is to depict the net pressure at the sharp gradient zone. In the asymptotic solutions, the net pressure at the sharp gradient zone is dominantly embodied by singular functions. For example, Π_s in Eqn (17) plays the dominant role in expressing the net pressure at the sharp gradient zone in the intermediate asymptotic solutions. These singular functions are introduced based on the analysis of the tip behaviors, and they depend on the fracture propagation regimes. In the numerical method, the net pressure in the sharp gradient zone is essentially approximated by linear functions. The domain lengths of the linear functions in the simulations are identical and equal 0.05 m because they are determined by the characteristic sizes of the elements along the fracture propagation path. Because of the constant ratio of l_t^{sp} to l_t, l_t^{sp} increases as the fracture propagates. The increasing l_t^{sp} leads to an increasing number of linear functions. The sharp gradient of the net pressure around the fracture tip can be well represented by the linear functions if a sufficient number are used. This is observed in Figure 11. The increasing number of linear functions results in an increasing accuracy for the numerical method, which is reflected by the decreasing relative errors as shown in Figure 13. Rather than taking special measures, the proposed numerical method approximates the tip behaviors by increasing the number of linear functions in a natural, continuous, and uniform manner.

DOI: 10.1002/nag

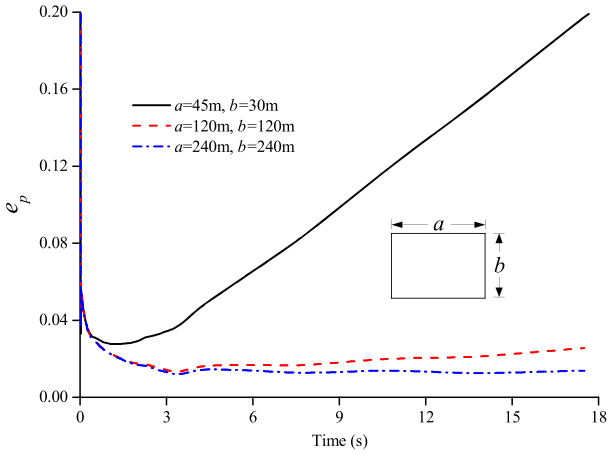

Figure 13. The e_ps for the viscosity-dominated examples without leak off.

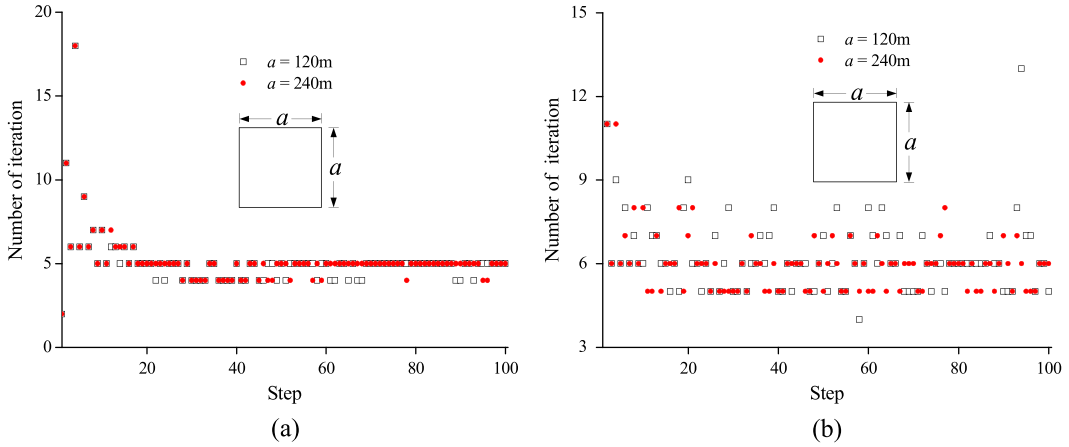

Figure 14. Number of iterations in the first 100 steps of the viscosity-dominated examples in the square models: (a) examples without leak off; (b) examples with leak off.

It is observed in Figure 11 that the fracture tip becomes more singular with decreasing K_m. This indicates that the examples in the viscosity-dominated case are harder to obtain convergence than those in other cases. The numbers of iterations needed to solve the nonlinear coupled Eqns (19) and (28) in the viscosity-dominated examples of the square models are plotted in Figure 14 for their first 100 steps. It is observed in Figure 14 that in most steps the solution obtains convergence within 10 iterations. This phenomenon is also observed in all other examples. The proposed method has excellent robustness.

6. CONCLUSIONS

In this paper, a uniform numerical method based on the finite element method is proposed to investigate hydraulic fracturing propagation regimes in the plane strain model. Similar to the asymptotic solutions, the numerical method is based on LEFM, lubrication theory, and Carter's leak-off model. Rather than taking special measures to capture the fracture behaviors in the sharp gradient zone, the numerical method simulates them by naturally and uniformly increasing functions. The energy dissipation regimes discussed using the numerical method range from viscosity-dominated to toughness-dominated regimes, with the fluid storage regimes ranging from

DOI: 10.1002/nag

zero-leak-off to small-leak-off regimes. The numerical method is verified by comparing the numerical results with the asymptotic solutions. The property of self-similarity in hydraulic fracturing is well expressed by the proposed numerical method. Domain size differences are an important source that leads to the differences between the asymptotic solutions and the numerical results. Even for examples in the viscosity-dominated case, the proposed numerical method exhibits excellent robustness.

APPENDIX A: ANALYTICAL SOLUTION FOR THE AUXILIARY FIELD

The auxiliary displacements in the local polar coordinates (r, θ), as shown in Figure 5, are [37]

$$\begin{aligned} u_1^a &= \frac{1}{2G}\sqrt{\frac{r}{2\pi}}\left[\cos\frac{\theta}{2}(\kappa - \cos\theta)\right] \\ u_2^a &= \frac{1}{2G}\sqrt{\frac{r}{2\pi}}\left[\sin\frac{\theta}{2}(\kappa - \cos\theta)\right] \end{aligned}, \tag{A.1}$$

where G is the shear modulus and κ is the Kosolov constant, which equals $3-4\nu$ in the plane strain model. The auxiliary stresses [37] are

$$\begin{aligned} \sigma_{11}^a &= \frac{1}{\sqrt{2\pi r}}\left\{\cos\frac{\theta}{2}\left[1 - \sin\frac{\theta}{2}\sin\frac{3\theta}{2}\right]\right\} \\ \sigma_{22}^a &= \frac{1}{\sqrt{2\pi r}}\left\{\cos\frac{\theta}{2}\left[1 + \sin\frac{\theta}{2}\sin\frac{3\theta}{2}\right]\right\} (-\pi \le \theta \le \pi)\,. \\ \sigma_{12}^a &= \sigma_{21}^a = \frac{1}{\sqrt{2\pi r}}\left\{\sin\frac{\theta}{2}\cos\frac{\theta}{2}\cos\frac{3\theta}{2}\right\} \end{aligned} \tag{A.2}$$

ACKNOWLEDGEMENTS

Funding for this project is provided by the Research Partnership to Secure Energy for America (RPSEA) through the 'Ultra-Deepwater and Unconventional Natural Gas and Other Petroleum Resources' program authorized by the US Energy Policy Act of 2005. RPSEA (www.rpsea.org) is a nonprofit corporation whose mission is to provide a stewardship role in ensuring the focused research, development, and deployment of safe and environmentally responsible technology that can effectively deliver hydrocarbons from domestic resources to the citizens of the USA. RPSEA, operating as a consortium of premier US energy research universities, industry, and independent research organizations, manages the program under a contract with the US Department of Energy's National Energy Technology Laboratory. The first author would like to thank Prof. Detournay and Dr Garagash for providing some original data in the asymptotic solutions.

REFERENCES

1. Lister JR. Buoyancy-driven fluid fracture: the effects of material toughness and of low-viscosity precursors. *Journal of Fluid Mechanics* 1990; **210**:263–280.
2. Levasseur S *et al.* Hydro-mechanical modelling of the excavation damaged zone around an underground excavation at Mont Terri Rock Laboratory. *International Journal of Rock Mechanics and Mining Sciences* 2010; **47**(3):414–425.
3. Hayashi K, Haimson BC. Characteristics of shut-in curves in hydraulic fracturing stress measurements and determination of in situ minimum compressive stress. *Journal of Geophysical Research* 1991; **96**(B11):18311–18321.
4. Murdoch LC. Mechanical analysis of ideaized shallow hydraulic fracture. *Journal of Geotechnical and Geoenvironmental Engineering* 2002; **128**(6):289–313.
5. Legarth B, Huenges E, Zimmermann G. Hydraulic fracturing in sedimentary geothermal reservoir: results and implications. *International Journal of Rock Mechanics and Mining Sciences* 2005; **42**(7-8):1028–1041.
6. Economides MJ, Nolte KG. *Reservoir Simulation* (3rd edn.). Wiley: Chichester, UK, 2000.
7. Adachi J, Detournay E. Plane strain propagation of a hydraulic fracture in a permeable rock. *Engineering Fracture Mechanics* 2008; **75**:4666–4694.
8. Geertsma J, Klerk F. Rapid method of predicting width and extent of hydraulically induced fractures. *Journal of Petroleum Technology* 1969; **21**:1571–1581.

DOI: 10.1002/nag

9. Nordren RP. Propagation of a vertical hydraulic fracture. *SPE* 7834 1972; **12**(8):306–314.
10. Abe H, Mura T, Keer L. Growth-rate of a penny-shaped crack in hydraulic fracturing of rocks. *Journal of Geophysical Research* 1976; **81**(29):5335–5340.
11. Garagash D, Detournay E. Plane-strain propagation of a fluid-driven fracture: small toughness solution. *Journal of Applied Mechanics* 2005; **72**:916–928.
12. Garagash DI, Detournay E, Adachi JI. Multiscale tip asmyptotics in hydraulic fracture with leak-off. *International Journal of Fluid Mechanics* 2011; **669**:260–297.
13. Garagash DI. Plain-strain propagation of a fluid-driven fracture during injection and shut-in: Asymptotics of large toughness. *Engineering Fracture Mechanics* 2006; **73**:456–481.
14. Bunger AP, Detournay E, Garagash DI. Toughness-dominated hydraulic fracture with leak-off. *International Journal of Fracture* 2005; **134**:175–190.
15. Hu J, Garagash DI. Plane-strain propagation of a fluid-driven crack in a permeable rock with fracture toughness. *ASCE Journal of Engineering Mechanics* 2010; **136**(9):1152–1166.
16. Adachi J, Detournay E. Self-similar solution of a plane-strain fracture driven by a power-law fluid. *International Journal for Numerical and Analytical Methods in Geomechanics* 2002; **26**:579–604.
17. Spence DA, Sharp PW. Self-similar solution for elastohydrodynamic cavity flow. *Proceedings of the Royal Society A: Mathematical, Physical and Engineering Sciences* 1985; **400**:289–313.
18. Adachi J. *Fluid-Driven Fracture in Permeable Rock*. University of Minnesota: Minneapolis, 2001.
19. Zhang X, Jeffrey RG, Thiercelin M. Mechanics of fluid-driven fracture growth in naturally fractured reservoirs with simple network geometries. *Journal of Geophysical Research* 2009; **114**:B12406.
20. Vandamme L, Roegiers J. Poroelasticity in hydraulic fracturing simulators. *Journal of Petroleum Technology* 1990; **42**(9):1199–1203.
21. Ouyang S, Carey GF, Yew CH. An adatpive fininte element scheme for hydraulic fracturing with proppant transport. *International Journal for Numerical Methods in Fluids* 1997; **24**(7):645–670.
22. Kresse O *et al.* Numerical modeling of hydraulic fractures interaction in complex naturally fractured formations. *Rock Mechanics and Rock Engineerig* 2013; **46**(3):555–568.
23. Devloo PRB *et al.* A finite element model for three dimensional hydraulic fracturing. *Mathematics and Computers in Simulation* 2006; **73**:142–155.
24. Sneddon IN, Lowengrub M. *Crack Problems in the Classical Theory of Elasticity*. John Wiley & Sons: New York, 1969.
25. Lecampion B. An extended finite element method for hydraulic fracture problems. *Communications in Numerical Methods in Engineering* 2009; **25**(2):121–133.
26. Chen ZR *et al.* Cohesive zone finite element-based modeling of hydraulic fracturing. *Acta Mechanica Solida Sinica* 2009; **22**(5):443–452.
27. Chen Z. Finite element modelling of viscosity-dominated hydraulic fractures. *Journal of Petroleum Science and Engineering* 2012; **88-89**:136–144.
28. Carrier B, Granet S. Numerical modeling of hydraulic fracture problem in permeable medium using cohesive zone model. *Engineering Fracture Mechanics* 2012; **79**:312–328.
29. Dugdale DS. Yielding of steel sheets containing slits. *Journal of the Mechanics and Physics of Solids* 1960; **8**:100–104.
30. Simulia. *Abaqus Theory Manual Ver 6.11*. Simulia: Providence, 2011.
31. Hunsweck MJ, Shen YX, Adrian JL. A finite element approach to the simulation of hydraulic fractures with lag. *International Journal of Numerical and Analytical Methods in Geomechanics* 2012; **37**(9):993–1015.
32. Batchelor GK. *An Introduction to Fluid Dynamics*. Cambridge University Press: Cambridge, UK, 1967.
33. Carter RD. Optimum fluid characteristics for fracture extension. In *Drilling and Production Practices*. American Petroelum Institute: Tulsa, 1957.
34. Irwin G. Analysis of stresses and strains near the end of a crack traversing a plate. *Journal of Applied Mechanics* 1957; **24**:361–364.
35. Spiegel MR, Lipschutz S, Spellman D. *Schaum's Outline of Vector Analysis* (2nd edn.). McGraw Hill: USA, 2009.
36. Abramowitz M, Stegun IA. *Handbook of Mathematical Functions*. Dover: New York, 1972.
37. Yau JF, Wang SS, Corten HT. A Mixed-mode crack analysis of isotropic solids using conservation laws of elasticity. *Journal of Applied Mechanics* 1980; **47**(2):335–341.
38. Fu P, Johnson SM, Carrigan CR. An explicitly coupled hydro-geomechanical model for simulating hydraulic fracturing in arbitrary discrete fracture networks. *International Journal for Numerical and Analytical Methods in Geomechanics* 2012; **37**:2278–2300.
39. Shen Y. A variational inequality formulation to incorporate the fluid lag in fluid-driven fracture propagation. *Computer Methods in Applied Mechanics and Engineering* 2014; **272**:17–33.
40. Press WH *et al. Numerical Recipes in Fortran: The Art of Scientific Computing*. Cambridge University Press: New York, 1992.
41. Adachi J *et al.* Computer simulation of hydraulic fractures. *International Journal of Rock Mechanics and Mining Sciences* 2007; **44**(5):739–757.

DOI: 10.1002/nag